Journal of Mathematical Biology manuscript No.
(will be inserted by the editor)

Vittorio Cristini · John Lowengrub · Qing Nie

Nonnecrotic tumor growth and the effect of vascularization

I. Linear analysis and self-similar evolution

Received: date / Revised version: date

Abstract. In this paper, we revisit the linear analysis of the transient evolution of a perturbed tumor interface in two and three dimensions, following [12,14,6, 3]. In Part II [9], we will study the full nonlinear problem using boundary-integral simulations. The tumor core is nonnecrotic and no inhibitor chemical species are present. A new formulation is developed that demonstrates that tumor evolution is described by a reduced set of two parameters and is qualitatively unaffected by the number of spatial dimensions. One parameter is related to the rate of mitosis. The other describes the balance between vascularization and apoptosis (programmed cell-death).

Three regimes of growth are identified with increasing degrees of vascularization: low (diffusion dominated), moderate and high vascularization. We demonstrate that parameter ranges exist for which the tumor evolves self-similarly (i.e., shape invariant) in the first two regimes. In the diffusion-dominated regime, vascularization is weak or absent and self-similar evolution leads to a nontrivial dormant state [5,4]. In the second regime vascularization becomes significant with respect to apoptosis; self-similar growth is unbounded and is associated with critical conditions of vascularization. Away from these critical conditions, perturbations may either grow with respect to the unperturbed shape, and thus lead to invasive fingering into the external tissues and metastasization, or decay to zero. In the high-vascularization regime, we find that during unbounded growth the tumor shape always tends to the unperturbed shape and neither self-similar nor fingering evolution occur. This last result is in agreement with recent experimental observations [17] of *in vivo* tumor growth and angiogenesis, and suggests that

First and Second Authors: School of Mathematics, and Department of Chemical Engineering and Materials Science, University of Minnesota, Minneapolis MN 55455

Third Author: Department of Mathematics, University of California at Irvine, Irvine CA 92697

Send offprint requests to: John Lowengrub, School of Mathematics, University of Minnesota, 206 Church St., Minneapolis MN 55455

VC and JL acknowledge partial support from the National Science Foundation and the Minnesota Supercomputing Institute, and the hospitality of the Institute for Mathematics and its Applications. VC also acknowledges the support of the MSI through a Reseach Scholar Award. QN acknowledges support from grant DMS0074414 from the NSF.

Key words: Tumor growth – Linear stability analysis – Self-similarity

the metastatic growth of highly-vascularized tumors is associated to vascular and elastic anisotropies, which are not included in our model.

1. Introduction

Tumor growth is a fundamental scientific problem and has received considerable attention by the mathematics community (see for example the recent review papers [1,7,2]). Here we focus on the continuum scale and formulate the problem in terms of conservation laws for the nutrient and tumor-cell concentrations, using the model formulated in [12,5,10]. This model describes evolution of avascular and vascularized tumors, but not the angiogenetic transition between the two.

The tumor is treated as an incompressible fluid and tissue elasticity is neglected. Cell-to-cell adhesive forces are modeled by a surface tension at the tumor-tissue interface. The growth of tumor mass is governed by a balance between cell mitosis and apoptosis. The rate of mitosis depends on the concentration of nutrient and inhibitor chemical species, that obey diffusion-reaction equations in the tumor volume. The bulk source of chemical species is the blood. The concentration of capillaries in the tumor is assumed to be uniform as are the concentrations of chemical species in the external tissues. In this paper the mathematical model is analyzed for the case of nonnecrotic tumors (i.e., Phase I tumors) [5] with no inhibitor chemical species. These conditions apply to small-sized tumors, or when the nutrient concentrations in the blood and in the external tissues are high. We anticipate that such a model should over-predict growth away from these conditions.

In this paper, a new formulation is developed that demonstrates that tumor evolution is described by a reduced set of two parameters that characterize families of solutions. Evolution is qualitatively unaffected by the number of spatial dimensions. One parameter is related to the rate of mitosis. The other describes the balance between vascularization and apoptosis. Three regimes of growth are identified with increasing degrees of vascularization: low (diffusion dominated), moderate and high vascularization. Following the approach we developed in [8], we demonstrate using linear analysis that parameter ranges exist for which the tumor evolves self-similarly (i.e., shape invariant) in the first two regimes. These self-similar states separate stable- and unstable-growth paths. In the diffusion-dominated regime, vascularization is weak or absent and self-similar evolution leads to a nontrivial dormant state [5,4]. In the second regime vascularization becomes significant with respect to apoptosis; self-similar growth is unbounded and is associated with critical conditions of vascularization. Away from these critical conditions, perturbations may either grow with respect to the unperturbed shape, and thus lead to invasive fingering into the external tissues and metastasization, or decay to zero. In the high-vascularization regime, we find that during unbounded growth the tumor shape always tends to the unperturbed shape and neither self-similar nor fingering evolution occur.

This last result is in agreement with recent experimental observations [17] of *in vivo* angiogenesis and tumor growth in a isotropic sponge-like matrix, and suggests that the metastatic growth of highly-vascularized tumors is associated to vascular and elastic anisotropies, which are not included in our model.

In Sect. 2 our new formulation for nonnecrotic tumors is presented. In Sect. 3 analytic results for radially symmetric tumors are revisited and the regimes of growth are identified. Our linear analysis in two and three dimensions is presented in Sect. 4. In Sect. 5 self-similar tumor evolution is investigated. Our conclusions and directions for future work are in Sect. 6.

2. Nonnecrotic tumor growth

2.1. Governing equations

We consider a nonnecrotic tumor occupying a volume $\Omega(t)$. In the absence of inhibitor chemical species, following [12,5,10], the diffusion equation for the concentration $\sigma(\mathbf{x},t)$ of nutrient is

$$\frac{\partial \sigma}{\partial t} = D\nabla^2\sigma + \Gamma, \tag{1}$$

where D is the diffusion constant, and Γ is the rate at which nutrient is added to Ω.

The rate Γ incorporates all sources and sinks of nutrient in the tumor volume. Nutrient is supplied by the vasculature at a rate $\Gamma_B(\sigma,\sigma_B)$, where σ_B is the (uniform) concentration in the blood. The rate of consumption of nutrient by the tumor cells is $\lambda\cdot\sigma$, with λ uniform. The blood-tissue transfer rate is assumed to be linear:

$$\Gamma_B = -\lambda_B \cdot (\sigma - \sigma_B)\,, \tag{2}$$

where λ_B is uniform. Thus, the rate Γ is given by

$$\Gamma = -\lambda_B \cdot (\sigma - \sigma_B) - \lambda\ \sigma. \tag{3}$$

Modeling the tumor as an incompressible fluid, it follows that the velocity field $\mathbf{u}$ in Ω satisfies the continuity equation

$$\nabla \cdot \mathbf{u} = \lambda_P, \tag{4}$$

where λ_P is the cell-proliferation rate. We choose here the model

$$\lambda_P = s\ \sigma - \lambda_A, \tag{5}$$

which is linear with respect to the nutrient [5]. In (5), $s\ \sigma$ is the mitosis rate, and λ_A is the rate of apoptosis (s and λ_A are assumed to be uniform).

The velocity is assumed to obey Darcy's law [11]:

$$\mathbf{u} = -\mu\nabla p, \tag{6}$$

where μ is the (constant) cell mobility and $p(\mathbf{x}, t)$ is the pressure inside Ω.

The boundary condition for concentration at $\Sigma \equiv \partial\Omega$ is

$$(\sigma)_\Sigma = \sigma^\infty, \tag{7}$$

where σ^∞ is the nutrient concentration outside the tumor volume, assumed to be uniform. Pressure is assumed to satisfy the Laplace-Young boundary condition

$$(p)_\Sigma = \gamma\kappa, \tag{8}$$

where γ is the surface tension related to cell-to-cell adhesive forces, and κ is local curvature. Finally, the normal velocity $V = \mathbf{n} \cdot (\mathbf{u})_\Sigma$ at the tumor boundary (with outward normal $\mathbf{n}$) is

$$V = -\mu\ \mathbf{n} \cdot (\nabla p)_\Sigma . \tag{9}$$

2.2. Dimensionless formulation

Using the initial equivalent radius R_0 of the tumor and the boundary conditions (7)–(9), let the characteristic space, time and concentration scales be

$$|\mathbf{x}| \sim R_0, \qquad t \sim \tau_\gamma, \qquad \sigma \sim \sigma^\infty, \tag{10}$$

where the surface tension time scale

$$\tau_\gamma = R_0^3/(\mu\gamma) \tag{11}$$

corresponds to the pressure scale $\hat{p} = \gamma/R_0$ and velocity scale $\hat{V} = \mu\gamma/R_0^2$.

We assume quasi-steady diffusion, $|\partial(\sigma/\sigma^\infty)/\partial(t/\tau_D)| \ll 1$, where the diffusion time scale

$$\tau_D = R_0^2/D. \tag{12}$$

This assumption [5] arises from the observation that the tumor doubling time scale (e.g., one day) is typically much larger that the diffusion time scale $\tau_D \approx$ one minute. The dimensionless form of the diffusion equation (1) is then

$$0 = \nabla^2\sigma + S\ \Gamma. \tag{13}$$

Note that in this equation and hereafter the same notation as in Sect. 2.1 is used for all the dimensionless equations. The relative strength of bulk source terms to diffusion is described by the dimensionless group

$$S = \frac{\tau_D}{\tau_\Gamma}. \tag{14}$$

The time scale associated with the source terms is

$$\tau_\Gamma = \sigma^\infty/\hat{\Gamma}, \tag{15}$$

where the characteristic rate of bulk supply is $\hat{\Gamma} = |\lambda_B \cdot (\sigma^\infty - \sigma_B) + \lambda\ \sigma^\infty|$.

The dimensionless form of equation (3) is

$$\Gamma = -L_B \cdot (\sigma - \chi_B) - L\ \sigma, \tag{16}$$

where the groups

$$L_B = \tau_\Gamma \ \lambda_B, \qquad L = \tau_\Gamma \ \lambda, \tag{17}$$

and

$$\chi_B = \frac{\sigma_B}{\sigma^\infty}. \tag{18}$$

The dimensionless form of the continuity equation (4) is

$$\nabla \cdot \mathbf{u} = G \ \lambda_P, \tag{19}$$

where the relative strength of cell proliferation and surface-tension-driven relaxation is

$$G = \tau_\gamma \ \hat{\lambda}_P, \tag{20}$$

and the characteristic proliferation rate is $\hat{\lambda}_P = |s \ \sigma^\infty - \lambda_A|$. The dimensionless form of equation (5) is then

$$\lambda_P = L_s \ \sigma - L_A, \tag{21}$$

where

$$L_s = \frac{s \ \sigma^\infty}{\hat{\lambda}_P}, \qquad L_A = \frac{\lambda_A}{\hat{\lambda}_P}. \tag{22}$$

Finally, the dimensionless forms of equations (6)–(9) are

$$\begin{aligned} \mathbf{u} &= -\nabla p, \\ (\sigma)_\Sigma &= 1, \\ (p)_\Sigma &= \kappa, \\ V &= -\mathbf{n} \cdot (\nabla p)_\Sigma. \end{aligned} \tag{23}$$

2.3. New formulation

By using algebraic manipulations, it can be shown that the dimensionless problem stated in Sect. 2.2 can be reformulated in terms of two decoupled problems:

$$\begin{aligned} \bar{\nabla}^2 \bar{\Gamma} - \bar{\Gamma} &= 0, \\ \left(\bar{\Gamma}\right)_\Sigma &= 1; \end{aligned} \tag{24}$$

and

$$\begin{aligned} \bar{\nabla}^2 q &= 0, \\ (q)_\Sigma &= \bar{\kappa} - \bar{L}_A \ \bar{G} \ \frac{(\bar{\mathbf{x}} \cdot \bar{\mathbf{x}})_\Sigma}{2d}, \end{aligned} \tag{25}$$

in a d–dimensional tumor. The interface Σ is evolved using

$$\bar{V} = -\mathbf{n} \cdot \left(\bar{\nabla} q\right)_\Sigma + \bar{G} \ \mathbf{n} \cdot \left(\bar{\nabla} \bar{\Gamma}\right)_\Sigma - \bar{L}_A \ \bar{G} \ \frac{\mathbf{n} \cdot (\bar{\mathbf{x}})_\Sigma}{d}. \tag{26}$$

The instantaneous problem stated above has only two dimensionless parameters:

$$\bar{G} = \frac{G\ L_s}{S^{\frac{3}{2}}}\ \frac{1-\chi_B\ L_B/(L_B+L)}{(L_B+L)^{\frac{3}{2}}},$$
$$\bar{L}_A = \frac{L_A/L_s - \chi_B\ L_B/(L_B+L)}{1-\chi_B\ L_B/\left(L_B+L\right)}. \tag{27}$$

Note that the parameter $\bar{L}_A = 3\Lambda$, where Λ is defined in [5].

Space and time have been rescaled as:

$$\bar{\mathbf{x}} = S^{\frac{1}{2}}\left(L_B+L\right)^{\frac{1}{2}}\mathbf{x}, \qquad \bar{t} = S^{\frac{3}{2}}\left(L_B+L\right)^{\frac{3}{2}}t. \tag{28}$$

Note that this implies that space and time are made dimensionless with the intrinsic scales $D^{\frac{1}{2}}\left(\lambda_B+\lambda\right)^{-\frac{1}{2}}$ and $D^{\frac{3}{2}}\left(\lambda_B+\lambda\right)^{-\frac{3}{2}}(\mu\gamma)^{-1}$, respectively. The variables $\bar{\Gamma}$ and q and the physical variables Γ, σ and p are related by the following formulas:

$$\Gamma = -\left(L_B+L-\chi_B\ L_B\right)\ \bar{\Gamma},$$
$$\sigma = 1-\left(1-\frac{\chi_B\ L_B}{L_B+L}\right)\left(1-\bar{\Gamma}\right),$$
$$p = S^{\frac{1}{2}}\left(L_B+L\right)^{\frac{1}{2}}\left(q+\left(1-\bar{\Gamma}\right)\ \bar{G}+\bar{L}_A\ \bar{G}\ \frac{\bar{\mathbf{x}}\cdot\bar{\mathbf{x}}}{2d}\right). \tag{29}$$

We define the rescaled rate of change of tumor volume $\bar{H} = \int_\Omega \mathrm{d}\bar{\mathbf{x}}^d$ as the mass flux $\bar{J} = \frac{\mathrm{d}}{\mathrm{d}\bar{t}}\bar{H} = \int_\Sigma \bar{V}\,\mathrm{d}\bar{\mathbf{x}}^{d-1}$. By using (24a)–(25a) we obtain from (26):

$$\bar{J} = -\bar{G}\ \int_\Omega \bar{\Gamma}\ \mathrm{d}\bar{\mathbf{x}}^d - \bar{L}_A\ \bar{G}\ \bar{H}. \tag{30}$$

3. Regimes of growth

In order to identify the regimes of growth, we consider evolution of a tumor that remains radially symmetric. The interface Σ is an infinite cylinder of instantaneous radius $\bar{R}(\bar{t})$ for $d=2$, and a sphere of radius $\bar{R}(\bar{t})$ for $d=3$. We assume that all variables have only $\bar{r}$–dependence, where $\bar{r}$ is the polar coordinate. Equations (24)–(25) have the nonsingular solutions

$$\bar{\Gamma}(\bar{r},\bar{t}) = \begin{cases} \dfrac{I_0(\bar{r})}{I_0(\bar{R})}, & d=2, \\ \left(\dfrac{\sinh(\bar{R})}{\bar{R}}\right)^{-1}\dfrac{\sinh(\bar{r})}{\bar{r}}, & d=3, \end{cases} \tag{31}$$

and $q(\bar{r},t) = (d-1)\bar{R}^{-1} - \bar{L}_A\bar{G}\bar{R}^2/(2d)$. Note that $q(\bar{r},t)\equiv q(\bar{R},t)$, i.e., q is uniform across the tumor volume.

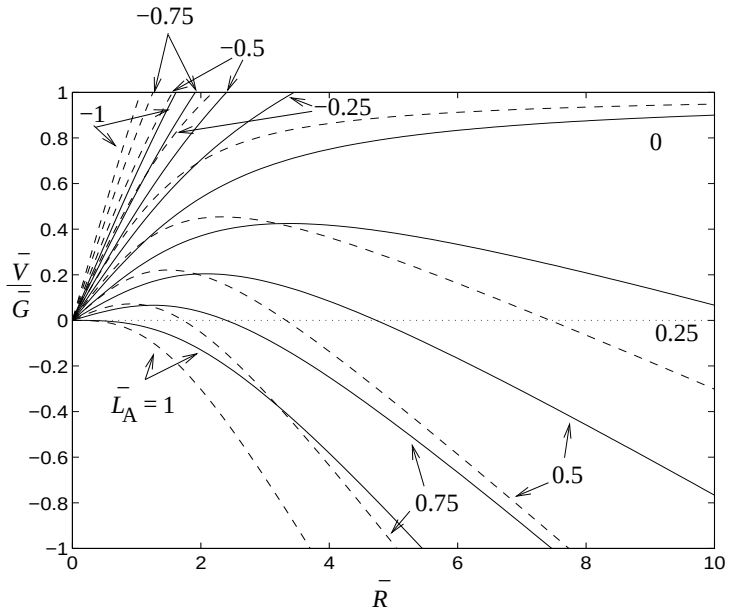

Fig. 1. Rescaled rate of growth $\bar{G}^{-1}\bar{V}$ from equation (32) as a function of rescaled tumor radius $\bar{R}$ for radially symmetric tumor growth and $d = 2$ (dashed) and 3 (solid); $\bar{L}_A$ labelled.

From equation (26) the evolution equation for the tumor radius $\bar{R}$ is:

$$\frac{\mathrm{d}\bar{R}}{\mathrm{d}\bar{t}} = \bar{V} = -\bar{G}\,\bar{L}_A\,\frac{\bar{R}}{d} + \bar{G}\,\begin{cases} \dfrac{I_1(\bar{R})}{I_0(\bar{R})}, & d = 2. \\ 1/\tanh(\bar{R}) - 1/\bar{R}, & d = 3. \end{cases} \tag{32}$$

Note that $|\bar{G}|$ rescales time and it can be shown that $\bar{V} = \bar{G} - \bar{L}_A\bar{G}\bar{R}$ for $d = 1$, where $\bar{R}$ is defined for $d = 1$ as the instantaneous position of the interface, with $\bar{R}(0) = 0$. The growth velocity is plotted for $d = 2,\ 3$ in figure 1. Note that, for $d = 3$, figures 1–2 correspond to figures 9 and 7, respectively, in [5]. They are included here for the sake of completeness. For given $\bar{L}_A$, evolution from initial condition $\bar{R}(0) = \bar{R}_0$ occurs along the corresponding curve. Three regimes are identified, and the behavior is qualitatively unaffected by the number of spatial dimensions d.

1. *Low vascularization*: $\bar{G} > 0$ and $\bar{L}_A > 0$. Evolution is monotonic and always leads to a stationary state $\bar{R}_\infty$, that corresponds to the intersection of the curves in figure 1 with the dotted line $\bar{V} = 0$. This behavior is in agreement with the experimental observations of *in vitro* diffusional growth [11] of multicell avascular spheroids to a dormant steady state [15,18]. Note that for $\chi_B = 0$, $\bar{G}, \bar{L}_A > 0$. For $d = 1$ the stationary state is identically $\bar{R}_\infty = \bar{L}_A^{-1}$.

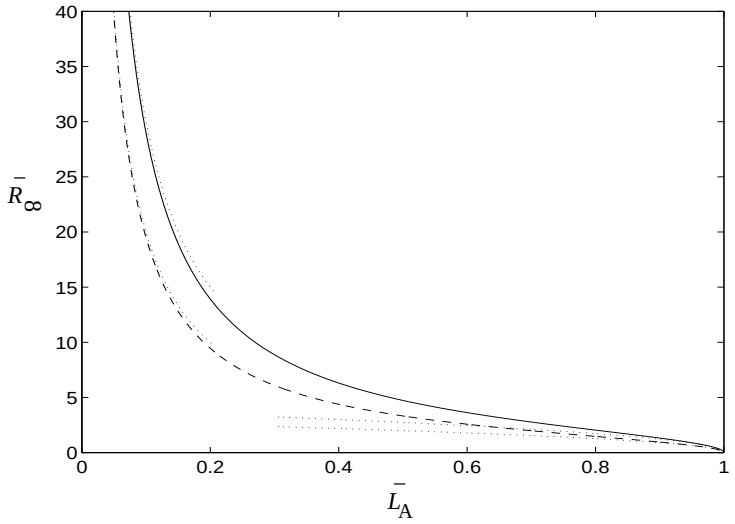

Fig. 2. Rescaled stationary radius $\bar{R}_\infty$ solution of equation (32) with $\bar{V} = 0$ as a function of $\bar{L}_A$ for $d = 2$ (dashed) and $d = 3$ (solid), and limiting behaviors (dotted) from equations (33). No stationary solution exists for $\bar{L}_A < 0$; $\bar{R}_\infty = 0$ identically for $\bar{L}_A > 1$.

2. *Moderate vascularization*: $\bar{G} > 0$ and $\bar{L}_A \leq 0$. Unbounded growth occurs from any initial radius $\bar{R}_0 > 0$. The growth tends to exponential for $\bar{L}_A < 0$ with velocity $\bar{V} \approx -\bar{L}_A \bar{G} \bar{R}/d$ as $\bar{R} \to \infty$, and to linear for $\bar{L}_A = 0$ with velocity $\bar{V} \approx \bar{G}$ as $\bar{R} \to \infty$.
3. *High vascularization*: $\bar{G} < 0$. Growth ($\bar{V} > 0$) may occur for $\bar{L}_A > 0$ and is always unbounded; for $\bar{L}_A < 0$ (for which cell apoptosis is dominant: $\bar{L}_A/\bar{L}_s > \chi_B L_B/(L_B + L)$), the evolution is always to the only stationary solution $\bar{R}_\infty = 0$. This stationary solution may also be achieved for $\bar{L}_A > 0$.

The stationary radius $\bar{R}_\infty$ is independent of $\bar{G}$, and is solution of $\bar{V} = 0$ with $\bar{V}$ from equation (32). The solution is plotted in figure 2. The stationary radius has limiting behaviors

$$\begin{aligned} &\bar{R}_\infty \to d\, \bar{L}_A^{-1}, \quad \bar{L}_A \to 0, \\ &\bar{R}_\infty \to d^{\frac{1}{2}} (d+2)^{\frac{1}{2}} \left(1 - \bar{L}_A\right)^{\frac{1}{2}}, \quad \bar{L}_A \to 1, \end{aligned} \tag{33}$$

where $\bar{R}_\infty$ vanishes. For $d = 1$ the stationary radius is $\bar{R}_\infty = \bar{L}_A^{-1}$ identically.

Pressure $\bar{p}_C = S^{-\frac{1}{2}} (L_B + L)^{-\frac{1}{2}} p(0,t)$ at the center of the tumor ($\bar{r} \equiv 0$) is obtained from equation (29c):

$$\bar{p}_C = \frac{d-1}{\bar{R}} + \bar{G} - \bar{L}_A\, \bar{G}\, \frac{\bar{R}^2}{2d} - \bar{G} \begin{cases} 1/I_0(\bar{R}), & d = 2, \\ \bar{R}/\sinh(\bar{R}), & d = 3, \end{cases} \tag{34}$$

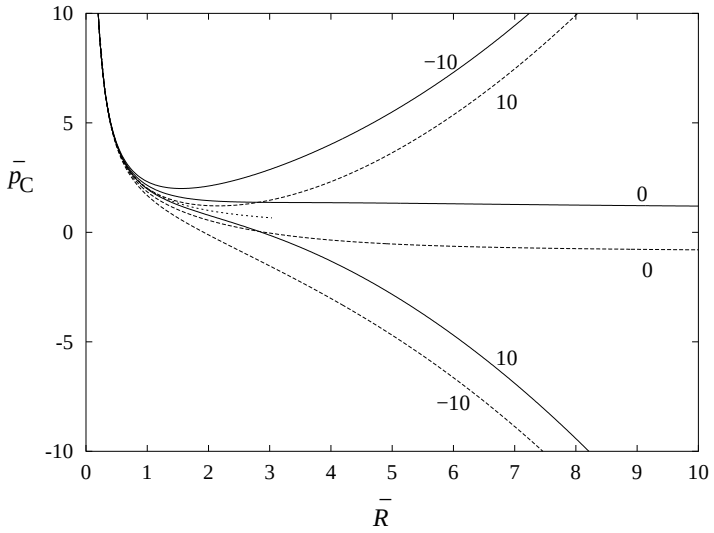

Fig. 3. Rescaled pressure $\bar{p}_C$ at the tumor's center from equation (34) as a function of the tumor's instantaneous radius $\bar{R}$ for $d = 3$; $\bar{G} = 1$ (solid) and $\bar{G} = -1$ (dashed); $\bar{L}_A$ labeled. The limiting behavior $\bar{p}_C \approx 2/\bar{R}$ as $\bar{R} \to 0$ is also shown (dotted).

which has the asymptotic behavior $\bar{p}_C \approx -\bar{L}_A \bar{G} \bar{R}^2/(2d)$ as $\bar{R} \to \infty$, indicating that if the tumor grows unbounded ($\bar{L}_A \bar{G} \leq 0$) the pressure at the center also does (unless $\bar{L}_A = 0$). This is a direct consequence of the absence of a necrotic core in this model. In a real system, the increasing pressure should itself contribute to necrosis [16]. It is known (see, for example, [7]) that tumor cells continuously replace the loss of cell volume in a tumor's core because of necrosis, thus maintaining pressure finite. In contrast for $\bar{L}_A \bar{G} \geq 0$ pressure is negative at large enough radii. For tumors that shrink to a point, pressure diverges as $\bar{p}_C \approx (d-1)/\bar{R}$ as $\bar{R} \to 0$. The pressure at the center is plotted in figure 3. For $d = 1$ we define $\bar{p}_C$ as the limit of $\bar{p}$ as $\bar{R} \to -\infty$, and it can be shown that $\bar{p}_C = \bar{G}$.

4. Linear analysis

We consider a perturbation of the spherical tumor interface Σ:

$$\bar{R}(\bar{t}) + \bar{\delta}(\bar{t}) \begin{cases} \mathrm{e}^{\mathrm{i}l\theta}, & d = 2, \\ Y_{l,m}(\theta, \phi), & d = 3, \end{cases} \tag{35}$$

where $\bar{\delta}$ is the dimensionless perturbation size and $Y_{l,m}$ is a spherical harmonic, where l and θ are polar wavenumber and angle, and m and ϕ azimuthal wavenumber and angle.

By solving the system of equations (24)–(26) on the perturbed interface we obtain the evolution equation (32) for the unperturbed radius $\bar{R}$ and the evolution equation for the perturbation size $\bar{\delta}$:

$$\bar{\delta}^{-1}\ \frac{\mathrm{d}\bar{\delta}}{\mathrm{d}\bar{t}} =$$

$$\begin{cases} l\cdot\left(\dfrac{\bar{J}}{2\pi\bar{R}^2}+\bar{L}_A\ \bar{G}\right)-\dfrac{\bar{L}_A\ \bar{G}}{2}+ \\ \bar{G}-\left(\dfrac{\bar{J}}{2\pi\bar{R}}+\bar{L}_A\ \bar{G}\ \dfrac{\bar{R}}{2}\right)\dfrac{I_{l-1}(\bar{R})}{I_l(\bar{R})}-\dfrac{l\left(l^2-1\right)}{\bar{R}^3}-\dfrac{\bar{G}\ I_1(\bar{R})}{\bar{R}\ I_0(\bar{R})}, \quad d=2, \\ \\ \bar{G}-\bar{L}_A\ \bar{G}-\dfrac{(l+2)\ \bar{J}}{4\pi\bar{R}^3}-\dfrac{l(l-1)(l+2)}{\bar{R}^3}, \qquad d=3, \end{cases} \tag{36}$$

where the dimensionless flux

$$\bar{J}=2\pi\,(d-1)\,\bar{R}^{d-1}\ \bar{V}+O\left(\bar{\delta}/\bar{R}\right)^2, \tag{37}$$

with $\bar{V}$ given by (32). Note that the linear evolution of perturbation is independent of the azimuthal wavenumber m. Also, for $d=1$ it can be shown that $\bar{\delta}^{-1}\frac{\mathrm{d}}{\mathrm{d}\bar{t}}\bar{\delta}=-l^3-\bar{G}\cdot\left(\left(l^2+1\right)^{\frac{1}{2}}-1\right)+\bar{L}_A\bar{G}\cdot\left(l\bar{R}-1\right)$. During unbounded growth, perturbations decay to zero for $d=1,2$ since $\bar{\delta}^{-1}\frac{\mathrm{d}}{\mathrm{d}\bar{t}}\bar{\delta}\approx l\bar{L}_A\bar{G}\bar{R}<0$ for $d=1$ and $\bar{\delta}^{-1}\frac{\mathrm{d}}{\mathrm{d}\bar{t}}\bar{\delta}\approx(l-1)\bar{L}_A\bar{G}/2<0$ for $d=2$, as $\bar{R}\to\infty$. For $d=3$, $\bar{\delta}^{-1}\frac{\mathrm{d}}{\mathrm{d}\bar{t}}\bar{\delta}\to 0$, as $\bar{R}\to\infty$, for $\bar{L}_A=-3(l-1)^{-1}$, and perturbations grow (decay) for $\bar{L}_A$ larger (smaller) than this value.

4.1. Nontrivial stationary states

Let us consider the evolution of a perturbation of a stationary radius $\bar{R}_\infty$. The stationary radius is solution of (32) with $\bar{V}=0$ and was plotted in figure 2 as a function of $0<\bar{L}_A<1$. Thus, $\bar{J}=0$ and equation (36) gives that there exists a critical

$$\bar{G}_l=\begin{cases} \bar{R}_\infty^{-3}\ \dfrac{2l\left(l^2-1\right)}{2+\bar{L}_A\left(2(l-1)-\bar{R}_\infty\ I_{l-1}(\bar{R}_\infty)/I_l(\bar{R}_\infty)\right)}, & d=2 \\ \\ \bar{R}_\infty^{-3}\ \dfrac{l\,(l-1)\,(l+2)}{1-\bar{L}_A}, \qquad d=3 \end{cases} \tag{38}$$

such that for $\bar{G}=\bar{G}_l>0$ (regime of low vascularization) the perturbation also remains stationary. It can be shown that, for both $d=2$ and 3, $\bar{G}_l>0$ for $\bar{R}_\infty>0$ and a perturbed stationary shape always exists. The perturbation grows unbounded for $\bar{G}>\bar{G}_l$ and decays to zero for $\bar{G}<\bar{G}_l$. At large radii $\bar{R}_\infty$, $\bar{G}_l\to 0$, thus in this limit perturbations always grow unbounded for $\bar{G}>0$. For $d=1$, we obtain $\bar{G}_l=l^3(1-\bar{L}_A+l-(1+l^2)^{\frac{1}{2}})^{-1}$, which indicates that a nontrivial stationary solution may not exist, since $\bar{G}_l$ can be negative.

5. Self-similar evolution

5.1. Constant microphysical parameters

The evolution of the perturbed shape is characterized by the shape factor $\bar{\delta}/\bar{R}$, governed by

$$\left(\bar{\delta}/\bar{R}\right)^{-1} \frac{\mathrm{d}}{\mathrm{d}\bar{t}} \left(\bar{\delta}/\bar{R}\right) = \bar{\delta}^{-1} \frac{\mathrm{d}\bar{\delta}}{\mathrm{d}\bar{t}} - \frac{\bar{J}}{2\pi\,(d-1)\,\bar{R}^d}. \tag{39}$$

Let us consider conditions for which the tumor grows unbounded. The asymptotic behavior of the flux $\bar{J}$ as $\bar{R} \to \infty$ is, from (32) and (37), $\bar{J} \approx -2\pi\,(d-1)\,\bar{L}_A \bar{G} \bar{R}^d/d$. Note that if the tumor grows unbounded then $\bar{L}_A \bar{G} \leq 0$.

For $d = 3$, it is easily shown from (36) and (39) that $\left(\bar{\delta}/\bar{R}\right)^{-1} \frac{\mathrm{d}}{\mathrm{d}\bar{t}} \left(\bar{\delta}/\bar{R}\right) \to \bar{G} \cdot \left(1 + \bar{L}_A l/3\right)$ as $\bar{R} \to \infty$ and there exists a critical

$$\bar{L}_{A,l} = -3l^{-1}, \tag{40}$$

such that for $\bar{L}_A = \bar{L}_{A,l}$ we obtain $\frac{\mathrm{d}}{\mathrm{d}\bar{t}} \left(\bar{\delta}/\bar{R}\right) \to 0$ as $\bar{R} \to \infty$, and the growing tumor tends to self-similar (shape invariant) evolution. Unbounded growth that tends to self-similar is possible only in the moderate-vascularization regime characterized by $\bar{G} > 0$ and $\bar{L}_A < 0$.

For $d = 2$, $\left(\bar{\delta}/\bar{R}\right)^{-1} \frac{\mathrm{d}}{\mathrm{d}\bar{t}} \left(\bar{\delta}/\bar{R}\right) \to \bar{L}_A \bar{G} l/2$ and is nonzero as $\bar{R} \to \infty$ for $\bar{L}_A \neq 0$ and constant. Thus self-similar long-time behavior is a peculiarity of three dimensions only. In two dimensions the perturbation decays to zero with respect to the underlying growing radius.

In the high-vascularization regime ($\bar{G} < 0$) with $\bar{L}_A > 0$, unbounded growth is characterized by a decay of the perturbation to zero with respect to the unperturbed radius for both $d = 2$ and 3. This is either an artifact of neglecting nonlinear effects (that will be explored in Part II [9]), or it is due to anisotropic distribution of the resistance of the external tissue to tumor growth, or to anisotropic distribution of blood vessels. It is known indeed that *carcinoma* evolve and metastasize by extending branches into regions of the external tissue where the mechanical resistance is lowest (e.g. [7]). Since in our model growth is overestimated, this result suggests that the formation of metastases in invasive tumors should be due to anisotropies rather than to vascularization alone. This conclusion is in agreement with recent experiments [17] of *in vivo* angiogenesis and tumor growth in a isotropic sponge-like matrix, where it is observed that under high-vascularization conditions the tumor mass, while expanding, maintains a compact spheroidal shape.

In figure 4 the evolution of perturbation during unbounded tumor growth ($\bar{R} \to \infty$) is examined in the moderate-vascularization regime characterized by $\bar{G} > 0$ and $\bar{L}_A \leq 0$. Corresponding to $d = 3$ and $\bar{L}_A = \bar{L}_{A,l}$ the shape tends to become self-similar. For $\bar{L}_A > \bar{L}_{A,l}$ the perturbation grows unbounded with respect to the unperturbed radius; for $\bar{L}_A < \bar{L}_{A,l}$ it decays

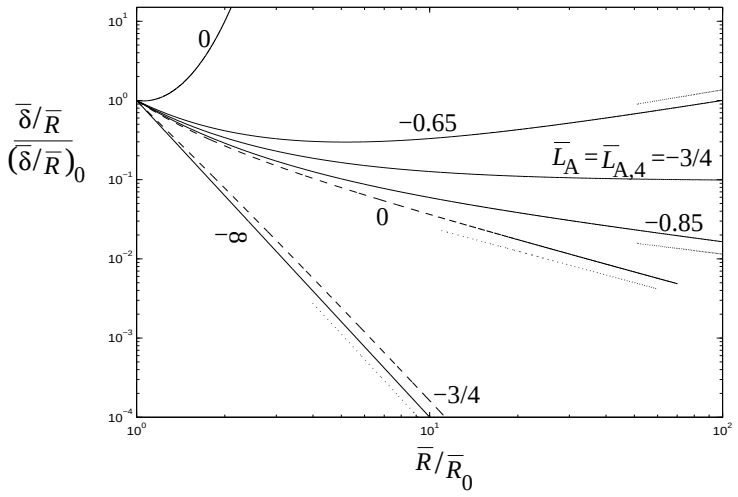

Fig. 4. Rescaled growth ratio $\left(\bar{\delta}/\bar{R}\right) / \left(\bar{\delta}/\bar{R}\right)_0$ as a function of rescaled radius $\bar{R}/\bar{R}_0$ during unbounded growth in the moderate-vascularization regime for $d = 2$ (dashed) and $d = 3$ (solid); $\bar{G} = 1$, $l = 4$, and $\bar{L}_A$ as labeled. The initial radius $\bar{R}_0 = 10$, except for the curve $d = 3$, $\bar{L}_A = 0$, for which $\bar{R}_0 = 7$. For this value of $\bar{L}_A$, $\bar{R}_0 = 7$ is above the maximum value of $\bar{R}$ for existence of a minimum in $\bar{\delta}/\bar{R}$. Asymptotic behaviors (dotted) from equations (41)–(42).

to zero. For $d = 2$ the perturbation always decays to zero. The behavior as $\bar{R} \to \infty$ is

$$\bar{\delta}/\bar{R} \sim \begin{cases} \bar{R}^{-l}, & d = 2, \\ \bar{R}^{-\left(3\bar{L}_A^{-1}+l\right)}, & d = 3, \end{cases} \tag{41}$$

for $\bar{L}_A \neq 0$, and

$$\bar{\delta}/\bar{R} \sim \begin{cases} \bar{R}^{-1}, & d = 2, \\ \mathrm{e}^{\bar{R}}, & d = 3, \end{cases} \tag{42}$$

independently of l, for $\bar{L}_A = 0$. Note that in this case $\bar{V} \to \bar{G}$ for both $d = 2$ and 3.

For $d = 3$ and $\bar{L}_A > \bar{L}_{A,l}$ there exists a minimum of $\bar{\delta}/\bar{R}$ which disappears for initial conditions $\bar{R}_0$ greater than a threshold value that depends on $\bar{L}_A$ and satisfies (43b). In figure 6, which is described further below, the threshold is given by the intersection between a curve $\bar{L}_A(\bar{R})$ with the line $\bar{L}_A = \text{constant} < 0$.

In figure 5 the limit $\left(\bar{\delta}/\bar{R}\right)_\infty$ of the growth ratio as $\bar{t} \to \infty$ is shown for conditions corresponding to self-similar evolution at $\bar{R} \to \infty$. The nontrivial limiting shape remains unchanged with respect to the initial condition for large initial unperturbed radius $\bar{R}_0$. As the three curves plotted indicate, the derivative (39) of the growth ratio scales $\sim l$ as $l \to \infty$.

In the low-vascularization regime ($\bar{G}, \bar{L}_A > 0$) and in the high-vascularization regime ($\bar{G} < 0$) with $\bar{L}_A < 0$, no unbounded growth occurs. In these regimes

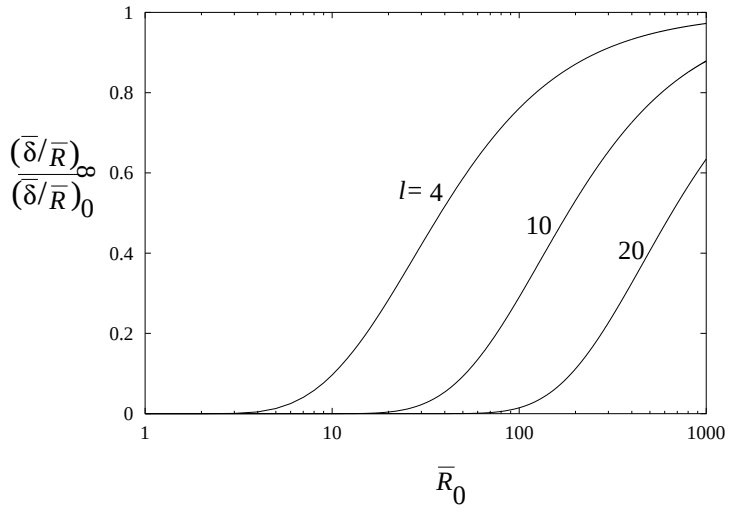

Fig. 5. Self-similar limit $\left(\bar{\delta}/\bar{R}\right)_\infty / \left(\bar{\delta}/\bar{R}\right)_0$ of the growth ratio rescaled with initial ratio, as a function of initial radius $\bar{R}_0$, for $\bar{R} \to \infty$ during unbounded growth in the moderate-vascularization regime; $d = 3$, $\bar{G} = 1$, l labelled, and $\bar{L}_A = \bar{L}_{A,l} = -3/l$.

the perturbation may either grow or decay, and thus in the first case complicated tumor morphologies can develop. This is illustrated by a full nonlinear simulation in figure 9 in Sect. 6.

5.2. Time-dependent parameters

In figure 6 (top) the apoptosis parameter $\bar{L}_A$ is shown as a function of unperturbed radius $\bar{R}$ during self-similar evolution:

$$\bar{L}_A = \begin{cases} \dfrac{2\left(l^2-1\right)}{\bar{G}\ \bar{R}^3} + 2l^{-1}\left(\dfrac{I_1\left(\bar{R}\right)\ I_{l-1}\left(\bar{R}\right)}{I_0\left(\bar{R}\right)\ I_l\left(\bar{R}\right)} - 1\right) \\ \qquad -2\left(1-2l^{-1}\right)\ \bar{R}^{-1}\ I_1\left(\bar{R}\right)/I_0\left(\bar{R}\right), \qquad d=2, \\ \dfrac{3\left(l+2\right)\left(l-1\right)}{\bar{G}\ \bar{R}^3} - 3l^{-1} \\ \qquad +3\left(1+3l^{-1}\right)\ \bar{R}^{-2}\ \left(\bar{R}/\tanh\left(\bar{R}\right)-1\right), \qquad d=3, \end{cases} \tag{43}$$

obtained by setting $\frac{\mathrm{d}}{\mathrm{d}\bar{t}}\left(\bar{\delta}/\bar{R}\right) = 0$ identically. For given $\bar{L}_A$ and $\bar{G}$, the above equations yield the threshold mode $l = l^*$ that evolves self-similarly at a given $\bar{R}$. Thus this threshold separates stable ($l > l^*$) and unstable ($l < l^*$) modes. For $\bar{L}_A \cdot \bar{G} > 0$ and $\left|\bar{L}_A\right|$ away from zero the two above formulas are well approximated by the first term (see (44) below), which gives, for

the threshold mode: $l^{*2} - 1 \approx \bar{L}_A \bar{G} \bar{R}^3/2$ for $d = 2$, and $(l^* + 2)(l^* - 1) \approx \bar{L}_A \bar{G} \bar{R}^3/3$ for $d = 3$.

The growth velocity corresponding to self-similar evolution, obtained from (32) with $\bar{L}_A$ given by (43), is plotted in figure 6 (bottom). The stationary states $\bar{R}_\infty$ correspond to the intersection of curves (43) with the curve plotted in figure 2, and replotted here. Figures 6 top and bottom indicate that in the low-vascularization (diffusion-dominated) regime ($\bar{G} > 0$, $\bar{L}_A > 0$) self-similar evolution towards a stationary state is not possible for $\bar{G}$ constant. For instance, the growth velocity $\bar{V} < 0$ for initial radius $\bar{R}_0 < \bar{R}_\infty$, and thus self-similar shrinkage of the tumor to zero occurs. On the other hand, for $\bar{R}_0 > \bar{R}_\infty$, $\bar{V} > 0$, and thus unbounded self-similar growth occurs. The limiting behaviors as $\bar{R} \to \infty$ are $\bar{L}_A \approx 2l^{-1}\bar{R}^{-1}$ for $d = 2$, and $\bar{L}_A \approx -3l^{-1} + 3\left(1 + 3l^{-1}\right)\bar{R}^{-1}$ for $d = 3$, and are independent of $\bar{G}$. For $d = 2$, self-similar evolution remains in the low-vascularization regime ($\bar{L}_A > 0$), and does not occur in the moderate-vascularization regime; in contrast, for $d = 3$, a transition takes place into the moderate-vascularization regime ($\bar{L}_A$ becomes negative), and leads to unbounded self-similar growth. As $l \to \infty$,

$$\bar{L}_A \to \begin{cases} 2\left(l^2 - 1\right)\ \bar{G}^{-1}\bar{R}^{-3}, & d = 2, \\ 3\left(l + 2\right)\left(l - 1\right)\ \bar{G}^{-1}\bar{R}^{-3}, & d = 3, \end{cases} \tag{44}$$

and thus $\bar{L}_A > 0$ and self-similar evolution in the low-vascularization regime becomes possible at all radii (and it becomes forbidden in the moderate-vascularization regime) also for $d = 3$.

Finally, in the high-vascularization regime ($\bar{G} < 0$), during self-similar evolution the velocity $\bar{V} < 0$. Thus shrinkage of a tumor from arbitrary initial condition to a point occurs, and self-similar unbounded growth is not possible.

The apoptosis parameter for self-similar evolution with $d = 1$ is $\bar{L}_A = \left(\bar{G}^{-1}l^3 - 1 + \left(l^2 + 1\right)^{\frac{1}{2}}\right)\left(l\bar{R} - 1\right)^{-1}$; note as a special case that, for $\bar{G} = l^{-3}\left(\left(1 + l^2\right)^{\frac{1}{2}} - 1\right)$, $\bar{L}_A = 0$ and unbounded self-similar growth occurs with constant parameters.

The value of $\bar{R}$ at which $\bar{L}_A = 0$ depends on $\bar{G}$ and l. In figure 7, this value of the radius is plotted as a function of $\bar{G}$. For given l and for $d = 3$, this value of $\bar{R}$ tends, for $\bar{G} \to \infty$, to a finite value $\bar{R}_l^*$ that is solution of (43b) with $\bar{L}_A = 0$ and $\bar{G} \to \infty$, and thus self-similar evolution in the low-vascularization regime remains possible for $\bar{R} < \bar{R}_l^*$. The asymptotic behavior is $\bar{R} - \bar{R}_l^* \sim \bar{G}^{-1}$. The value $\bar{R}_l^* \sim l$ for $l \to \infty$. For $\bar{G} \to 0^+$, $\bar{R} \approx \bar{G}^{-\frac{1}{3}} l^{\frac{1}{3}} \left(l + 2\right)^{\frac{1}{3}} \left(l - 1\right)^{\frac{1}{3}}$.

In the high-vascularization regime ($\bar{G} < 0$) for $d = 2$ the value of $\bar{R}$ for which $\bar{L}_A = 0$ increases as $\bar{R} \approx \left(-\bar{G}\right)^{-\frac{1}{2}} l^{\frac{1}{2}} \left(l^2 - 1\right)^{\frac{1}{2}}$ for $\bar{G} \to 0^-$ and vanishes as $\bar{R} \approx \left(-\bar{G}\right)^{-\frac{1}{3}} 2^{\frac{1}{3}} \left(l^2 - 1\right)^{\frac{1}{3}}$ for $\bar{G} \to -\infty$. In contrast, for $d = 3$ $\bar{L}_A < 0$ identically or it changes sign twice. The two corresponding values

of $\bar{R}$ have asymptotic behaviors, as $\bar{G} \to -\infty$, $\bar{R} \approx \bar{G}^{-\frac{1}{3}} 3^{\frac{1}{3}} (l+2)^{\frac{1}{3}} (l-1)^{\frac{1}{3}}$ and $\bar{R} - \bar{R}_l^* \sim \bar{G}^{-1}$.

The behaviors described remain qualitatively unchanged for different values of l, and the radius at which $\bar{L}_A = 0$ scales as $\bar{R} \sim l$ for $l \to \infty$.

To summarize, we found self-similar evolution in all regimes with varying $\bar{L}_A$ and constant $\bar{G}$. However, we discovered that in the low-vascularization regime, self-similar evolution to a steady state does not occur under these conditions. Similarly, self-similar unbounded growth in the high-vascularization regime does not occur.

Next, we examine the possibility of self-similar evolution enforced by varying $\bar{G}$ in addition to $\bar{L}_A$. In figure 8 (top) the values of growth parameter $\bar{G}$ as a function of radius $\bar{R}$ are plotted corresponding to nontrivial stationary states with a fixed tumor shape: $\frac{\mathrm{d}}{\mathrm{d}\bar{R}} \left(\bar{\delta}/\bar{R}\right) = 0$. In the high-vascularization regime ($\bar{G} < 0$), self-similar evolution occurs below the curves $\bar{V} = 0$ in figure 8 (top), and thus $\bar{V} < 0$ and self-similar unbounded growth is forbidden.

We consider then self-similar evolution between nontrivial stationary states in the low-vascularization regime ($\bar{G} > 0$). The dotted lines in figure 8 (top) represent an experiment in which $\bar{G}$ is varied linearly between a stationary state $\bar{R}_{\infty,1}$ and a stationary state $\bar{R}_{\infty,2} > \bar{R}_{\infty,1}$. In figure 8 (bottom), the corresponding growth velocities and time-dependent apoptosis parameters are shown. The figure reveals that during this experiment the growth velocity $\bar{V} > 0$ and thus self-similar evolution is possible between the two stationary states. Other experimental paths are possible, that lead to either growth or shrinkage of tumors to stationary states. The qualitative behaviors described are not affected by l.

6. Conclusions

In this paper (Part I of our study), we have revisited the linear analysis of the transient evolution of a perturbed nonnecrotic-tumor interface in two and three dimensions. A new formulation was developed that demonstrates that tumor evolution is described by a reduced set of two parameters and is qualitatively unaffected by the number of spatial dimensions. The parameters $\bar{G}$ and $\bar{L}_A$ are related to the rates of mitosis and apoptosis, respectively. Both parameters contain the effect of vascularization. The regimes of growth were identified to be: low (diffusion dominated), moderate and high vascularization. We demonstrated that parameter ranges exist for which the tumor evolves self-similarly in the first two regimes. self-similar solutions separate stable and unstable regimes of evolution of perturbations. Unstable regimes correspond to invasive fingering into the external tissues and metastasization.

In the diffusion-dominated regime, self-similar evolution leads to a nontrivial dormant state. We simulated an *in vitro* experiment of self-similar diffusional evolution, by varying the parameters $\bar{G}$ and $\bar{L}_A$. In the absence of vascularization ($\sigma_B = \lambda_B = 0$), the two dimensionless parameters (27)

reduce to

$$\bar{G} = \frac{sD^{\frac{3}{2}}}{\mu\gamma\lambda^{\frac{3}{2}}}\,\sigma^{\infty}, \qquad \bar{L}_A = \frac{\lambda_A}{s}\,1/\sigma^{\infty}. \tag{45}$$

Thus a physical experiment can be conducted in which it may be possible to observe self-similar growth in the laboratory, by varying the supply of nutrient σ^{∞}, above the minimum threshold below which necrosis occurs.

In the moderate-vascularization regime vascularization becomes significant with respect to apoptosis; self-similar growth is unbounded and is associated with critical conditions of vascularization. In contrast in the high-vascularization regime, we find that during unbounded growth the tumor shape always tends to the unperturbed shape and neither self-similar nor fingering evolution occur. This last result, in agreement with experimental observations [17], suggests that the metastatic growth of highly-vascularized tumors is associated to vascular and elastic anisotropies, which are not included in our model. Vascular anisotropies can be accounted for by introducing a nonuniform concentration σ_B of nutrient in the blood. This will be the subject of future investigation. Elastic anisotropies, that may set preferred directions of growth, will be accounted for by a more sophisticated model, which will include the elastic response of the tumor (e.g., [13]) and surrounding elastic tissue.

In Part II [9] we will contrast the analytic results presented in this paper to the results of full nonlinear simulation of the governing equations. A boundary-integral method will be used, and we will focus on the 2-D case, which is expected to contain all the qualitative features of the more physical 3-D case. The numerical model will include description of the topological transitions associated to the formation of metastases. In figure 9, an example of nonlinear simulation of unstable growth of perturbation in the low-vascularization regime is shown. The linear evolution is also shown (dashed). The linear theory predicts splitting and formation of two metastases at time $\bar{t} = 2.28$. In contrast, nonlinearity weakens this initial tendency towards splitting, through the creation of new modes, some of which become unstable at later times. Invasive fingering and the onset of metastasization (and reconnection) are evident.

References

1. J. Adam, General Aspects of Modeling Tumor Growth and Immune Response. *In: A Survey of Models on Tumor Immune Systems Dynamics, J. Adam and N. Bellomo Editors* (Birkhauser, Boston 1996) 15–87.
2. N. Bellomo and L. Preziosi, Modelling and Mathematical Problems Related to Tumor Evolution and Its Interaction with the Immune System. Mathl. Comput. Modelling **32,** (2000) 413–452.
3. H. M. Byrne, The importance of intercellular adhesion in the development of carcinomas. IMA J. Math. Med. Biol. **14,** (1997) 305–323.
4. H. M. Byrne, A weakly nonlinear analysis of a model of avascular solid tumour growth. J. Math. Biol. **39,** (1999) 59–89.
5. H. M. Byrne and M. A. J. Chaplain, Growth of Nonnecrotic Tumors in the Presence and Absence of Inhibitors. Mathl. Biosci. **130,** (1995) 151–181.

6. H. M. Byrne and M. A. J. Chaplain, Modelling the role of cell-cell adhesion in the growth and development of carcinomas. Mathl. Comput. Modelling **24,** (1996) 1–17.
7. M. A. J. Chaplain, Avascular growth, Angiogenesis and Vascular growth in Solid Tumours: The Mathematic Modelling of the Stages of Tumour Development. Mathl. Comput. Modelling **23,** (1996) 47–87.
8. V. Cristini and J. Lowengrub, Three-dimensional crystal growth. I. Linear analysis and self-similar evolution. Submitted to Physical Rev. E.
9. V. Cristini, J. Lowengrub and Q. Nie, Nonnecrotic tumor growth and the effect of vascularization. II. Nonlinear simulation. To be submitted to J. Math. Biol.
10. A. Friedman and F. Reitich, Analysis of a mathematical model for the growth of tumors. J. Math. Biol. **38,** (1999) 262.
11. H. P. Greenspan, Models for the Growth of a Solid Tumor by diffusion. Stud. Appl. Math. **LI,4,** (1972) 317–340.
12. H. P. Greenspan, On the growth and stability of cell cultures and solid tumors. J. Theor. Biol. **56,** (1976) 229–242.
13. A. F. Jones, H. M. Byrne, J. S. Gibson and J. W. Dold, A mathematical model of the stress induced during avascular tumour growth. J. Math. Biol. **40,** (2000) 473–499.
14. D. L. S. McElwain and L. E. Morris, Apoptosis as a volume loss mechanism in mathematical models of solid tumor growth. Math. Biosci. **39,** (1978) 147–157.
15. W. Mueller-Klieser, Multicellular spheroids: a review on cellular aggregates in cancer research. J. Cancer Res. Clin. Oncol. **113,** (1987) 101–122.
16. P. A. Netti. Personal communication.
17. J. E. Nor, J. Christensen, J. Liu, M. Peters, D. J. Mooney, R. M. Strieter and P. J. Polverini, Up-Regulation of Bcl-2 in Microvascular Endothelial Cells Enhances Intratumoral Angiogenesis and Accelerates Tumor Growth. Cancer Res. **61,** (2001) 2183–2188.
18. R. M. Sutherland, Cell and Environment interactions in tumor microregions: the multicell spheroid model. Science **240,** (1988) 177-184.

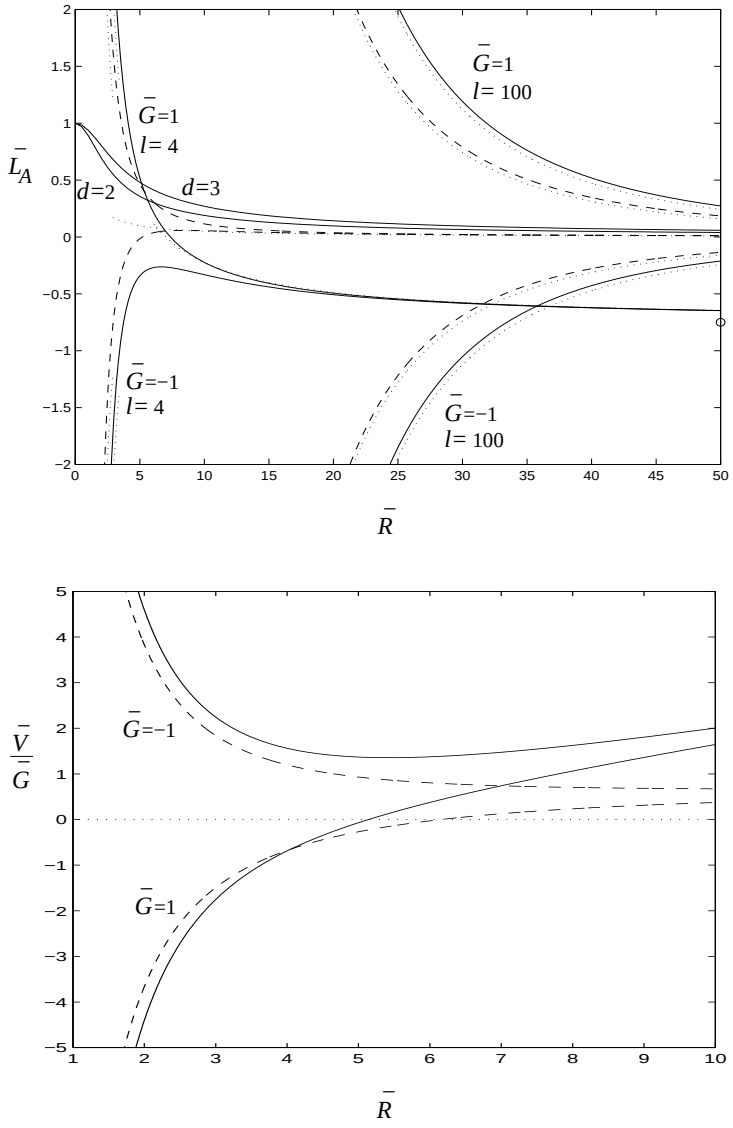

Fig. 6. Top: apoptosis parameter $\bar{L}_A$ as a function of unperturbed radius $\bar{R}$ from condition (43) for self-similar evolution; $d = 2$ (dashed) and $d = 3$ (solid); $\bar{G}$ and l labelled. Asymptotic behaviors (44) (dotted). The two solid curves labelled with values of d are reproduced from figure 2. Bottom: corresponding growth velocity $\bar{G}^{-1}\bar{V}$; $l = 4$.

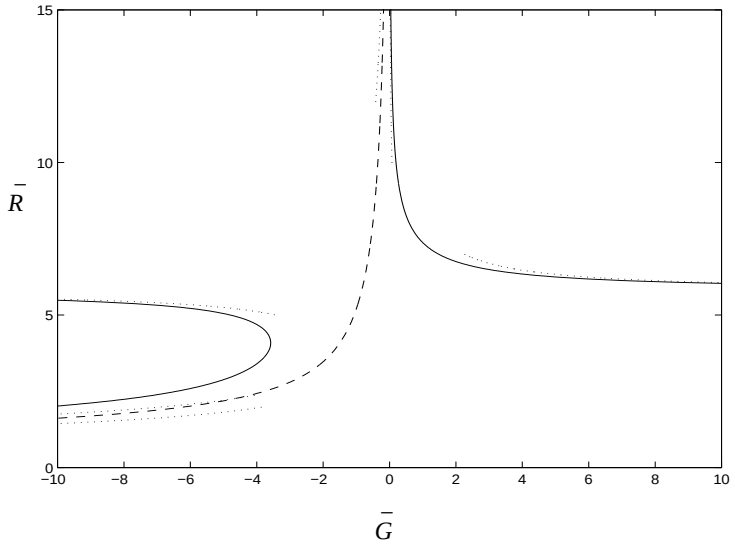

Fig. 7. Value of radius $\bar{R}$ at which $\bar{L}_A = 0$ from self-similarity condition (43), as a function of $\bar{G}$; $d = 2$ (dashed) and $d = 3$ (solid); $l = 4$. Asymptotic behaviors as in text (dotted).

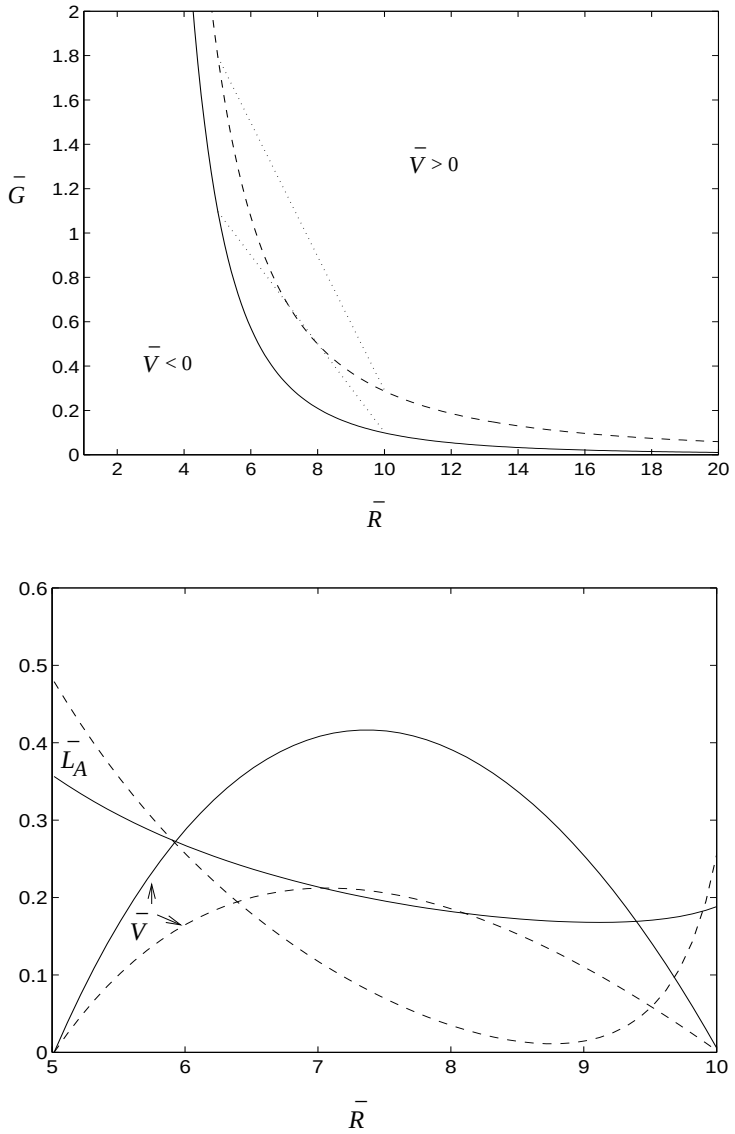

Fig. 8. Top: growth parameter $\bar{G}$ from condition (43) for shape invariance, with $\bar{V} = 0$ and $\bar{L}_A(\bar{R})$ from figure 2, as a function of radius $\bar{R}$; $d = 2$ (dashed) and $d = 3$ (solid); $l = 4$. Experiment of self-similar evolution between stationary states (dotted), with $\bar{G}$ imposed as a linear function of $\bar{R}$. Bottom: apoptosis parameter $\bar{L}_A$ from (43), and growth velocity $\bar{V}$, as a function of radius $\bar{R}$ during such experiment.

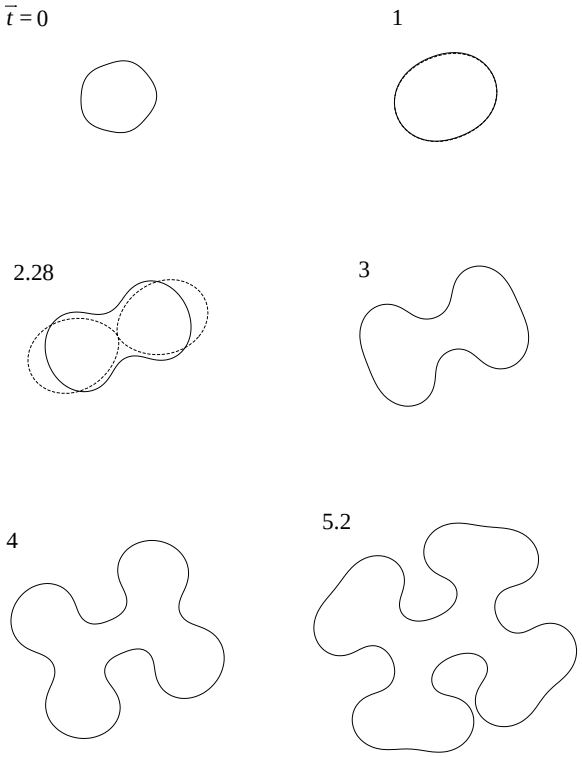

Fig. 9. Solid: nonlinear boundary-integral simulation of unstable growth of perturbation in the low-vascularization regime; $d = 2$, $\bar{G} = 20$, $\bar{L}_A = 0.6$, initial and stationary radii $\bar{R}_0 = 2$ and $\bar{R}_\infty = 2.5771$. Time is labeled, rescaled as in (28). Dashed: linear result for same conditions.